Article

Structural and Spectroscopic Characterization of a Charge-Separated Uranium Benzophenone Ketyl Radical Complex

Oanh P. Lam, Christian Anthon, Frank W. Heinemann, Joseph M. O'Connor, and Karsten Meyer

J. Am. Chem. Soc., **2008**, 130 (20), 6567-6576 • DOI: 10.1021/ja801007q • Publication Date (Web): 26 April 2008

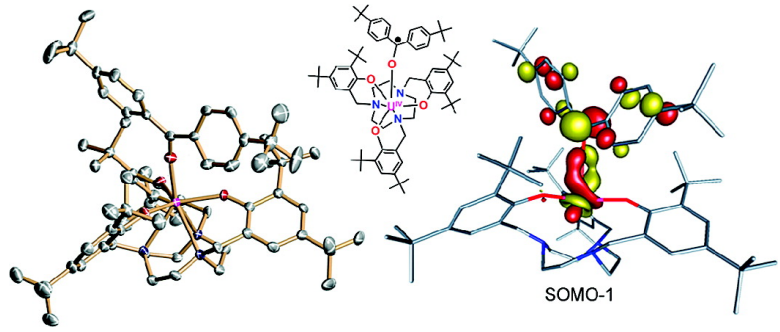

More About This Article

Additional resources and features associated with this article are available within the HTML version:

- Supporting Information
- Links to the 1 articles that cite this article, as of the time of this article download
- Access to high resolution figures
- Links to articles and content related to this article
- Copyright permission to reproduce figures and/or text from this article

View the Full Text HTML

J|A|C|S
ARTICLES

Published on Web 04/26/2008

Structural and Spectroscopic Characterization of a Charge-Separated Uranium Benzophenone Ketyl Radical Complex

Oanh P. Lam,[†,‡] Christian Anthon,[‡] Frank W. Heinemann,[‡] Joseph M. O'Connor,[†] and Karsten Meyer*[,‡]

Department of Chemistry, University of California, San Diego, 9500 Gilman Drive, La Jolla, California 92093, and Department of Chemistry and Pharmacy, Inorganic Chemistry, University of Erlangen-Nürnberg, Egerlandstr. 1, D-91058 Erlangen, Germany

Received February 8, 2008; E-mail: kmeyer@chemie.unierlangen.de

Abstract: The reaction of [(($^{t\text{-Bu}}$ArO)$_3$tacn)U^{III}] (**1**) with 4,4′-di-*tert*-butylbenzophenone affords a unique isolable U(IV) ketyl radical species [(($^{t\text{-Bu}}$ArO)$_3$tacn)U^{IV}(OC•$^{t\text{-Bu}}$Ph$_2$)] (**2**) supported by XRD data, magnetization measurements, and DFT calculations. Isolation and full characterization of the corresponding diphenyl methoxide complex [(($^{t\text{-Bu}}$ArO)$_3$tacn)U^{IV}(OCH$^{t\text{-Bu}}$Ph$_2$)] (**3**) is also presented. The one-electron reduction of benzophenone by [((^{Ad}ArO)$_3$tacn)U^{III}] (**4**) leads to a purple U(IV) ketyl radical intermediate [((^{Ad}ArO)$_3$tacn)U^{IV}(OC•Ph$_2$)] (**5**). This species is highly reactive, and attempts at isolation were unsuccessful and resulted in methoxide complex [((^{Ad}ArO)$_3$tacn)U^{IV}(OCHPh$_2$)] (**6**) from H abstraction and dinuclear para-coupled complex [((^{Ad}ArO)$_3$tacn)U^{IV}(OCPhPh−CPh$_2$O)U^{IV}((^{Ad}ArO)$_3$tacn)] (**7**).

Introduction

The syntheses of ketyl radicals through single-electron reduction of ketones with alkali metals were first discovered over 100 years ago.[1–3] Ever since, this class of compounds has attracted continuous attention in many areas, such as aiding in drying and deoxygenating solvents, serving as important intermediates in organic reactions,[4–6] and providing interesting sources for spectroscopic studies.[7–13] However, due to the highly reactive nature of ketyl radical species, isolation and structural characterization of benzophenone ketyl complexes have eluded scientists for many decades. The planar, fused-ring system in fluorenone ketyls permits more effective electron delocalization relative to that in benzophenone ketyls, and in 1995, Hou cleverly exploited this stabilization affect in the successful solid-state structural characterization of a samarium fluorenone ketyl complex.[14] Subsequent studies demonstrated that stable metal fluorenone ketyl complexes could be isolated in systems where the benzophenone analogues proved too unstable for solid-state characterization.[15–18]

Despite successes with the structural isolation of fluorenone ketyls, those of benzophenone ketyls are still sought after because they have shown to be much more reactive.[7,9,12,13] Attempts to isolate metal benzophenone ketyl radicals have often resulted in hydrogen abstraction to form metal alkoxides,[17,19] insertions into M−L bonds,[20–28] or reductive coupling to form

[†] University of California, San Diego.
[‡] University of Erlangen-Nürnberg.

(1) Bechman, F.; Paul, T. *Justus Liebigs Ann. Chem.* **1891**, *266*, 1.
(2) Schlenk, W.; Weickel, T. *Ber. Dtsch. Chem. Ges.* **1911**, *44*, 1182–1189.
(3) Schlenk, W.; Thal, A. *Ber. Dtsch. Chem. Ges.* **1913**, *46*, 2840–2854.
(4) Skrydstrup, T. *Angew. Chem., Int. Ed. Engl.* **1997**, *36*, 345–347.
(5) Molander, G. A. *Chem. Rev.* **1992**, *92*, 29–68.
(6) Molander, G. A.; Harris, C. R. *Chem. Rev.* **1996**, *96*, 307–338.
(7) Sakamoto, M.; Cai, X.; Fujitsuka, M.; Majima, T. *Chem.—Eur. J.* **2006**, *12*, 1610–1617.
(8) Anandhi, R.; Umapathy, S. *J. Raman Spectrosc.* **2000**, *31*, 331–338.
(9) Covert, K. J.; Wolczanski, P. T.; Hill, S. A.; Krusic, P. J. *Inorg. Chem.* **1992**, *31*, 66–78.
(10) Dams, R.; Malinowski, M.; Westdorp, I.; Geise, H. Y. *J. Org. Chem.* **1982**, *47*, 248–259.
(11) Mao, S. W.; Nakamura, K.; Hirota, N. *J. Am. Chem. Soc.* **1974**, *96*, 5341–5349.
(12) Hirota, N. *J. Am. Chem. Soc.* **1967**, *89*, 32–41.
(13) Hirota, N.; Weissman, S. I. *J. Am. Chem. Soc.* **1964**, *86*, 2538–2545.
(14) Hou, Z.; Miyano, T.; Yamazaki, H.; Wakatsuki, Y. *J. Am. Chem. Soc.* **1995**, *117*, 4421–4422.
(15) Hou, Z.; Jia, X.; Fujita, A.; Tezuka, H.; Yamazaki, H.; Wakatsuki, Y. *Chem.—Eur. J.* **2000**, *6*, 2994–3005.
(16) Hou, Z.; Fujita, A.; Koizumi, T.; Yamazaki, H.; Wakatsuki, Y. *Organometallics* **1999**, *18*, 1979–1985.
(17) Hou, Z.; Fujita, A.; Zhang, Y.; Miyano, T.; Yamazaki, H.; Wakatsuki, Y. *J. Am. Chem. Soc.* **1998**, *120*, 754–766.
(18) Hou, Z.; Fujita, A.; Yamazaki, H.; Wakatsuki, Y. *J. Am. Chem. Soc.* **1996**, *118*, 2503–2504.
(19) Adam, R.; Villiers, C.; Ephritikhine, M.; Lance, M.; Nierlich, M.; Vigner, J. *New J. Chem.* **1993**, *17*, 455.
(20) Ogoshi, S.; Tonomori, K.; Oka, M.; Kurosawa, H. *J. Am. Chem. Soc.* **2006**, *128*, 7077–7086.
(21) Vela, J.; Vaddadi, S.; Cundari, T. R.; Smith, J. M.; Gregory, E. A.; Lachicotte, R. J.; Flaschenriem, C. J.; Holland, P. L. *Organometallics* **2004**, *23*, 5226–5239.
(22) Basuli, F.; Tomaszewski, J.; Huffman, J. C.; Mindiola, D. J. *Organometallics* **2003**, *22*, 4705–4714.
(23) Emslie, D. J. H.; Piers, W. E.; Parvez, M.; McDonald, R. *Organometallics* **2002**, *21*, 4226–4240.
(24) Mindiola, D. J.; Cummins, C. C. *Organometallics* **2001**, *20*, 3626–3628.
(25) Castillo, I.; Tilley, T. D. *Organometallics* **2000**, *19*, 4733–4739.
(26) Liang, F.; Jacobsen, H.; Schmalle, H. W.; Fox, T.; Berke, H. *Organometallics* **2000**, *19*, 1950–1962.
(27) Breen, T. L.; Stephan, D. W. *Organometallics* **1996**, *15*, 4509–4514.
(28) Scholz, J.; Görls, H. *Inorg. Chem.* **1996**, *35*, 4378–4382.
(29) Fedushkin, I. L.; Skatova, A. A.; Cherkasov, V. K.; Chudakova, V. A.; Dechert, S.; Hummert, M.; Schumann, H. *Chem.—Eur. J.* **2003**, *9*, 5778–5783.

Scheme 1. Formation of U(IV) Benzophenone Ketyl Radical Complex **2** through a One-Electron Reduction of 4,4′-Di-*tert*-butylbenzophenone by U(III) Precursor Complex [(($^{t\text{-Bu}}$ArO)$_3$tacn)U^{III}] (**1**) Followed by H Abstraction To Form a U(IV) Diphenyl Methoxide Complex **3**

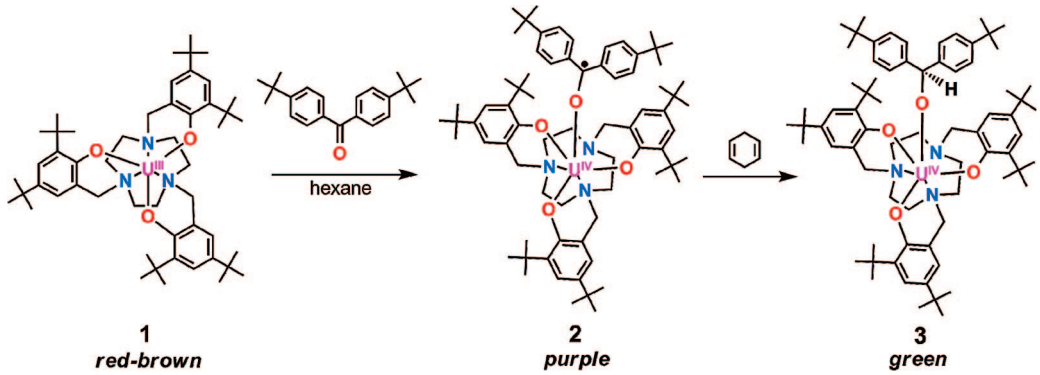

pinacolate complexes.[17,29–33] To date, the isolation and structural characterization of benzophenone ketyl radical complexes are limited to complexes of alkali/alkaline earth and samarium metals.[15,34–36] Here we demonstrate the use of a triazacyclononane-anchored trisaryloxide ligand chelated to uranium to stabilize a charge-separated di-*tert*-butyl benzophenone ketyl radical species. In addition to X-ray diffraction, this complex has been characterized by electronic absorption spectroscopy, combustion analysis, magnetism, and DFT studies. Preliminary reactivity studies on the uranium ketyl complexes have led to the formation of a U(IV) diphenyl methoxide complex via H-atom abstraction chemistry and the first crystallographic evidence of dimer formation resulting from a head-to-tail reductive para coupling of two benzophenone ketyl ligands.

Results and Discussion

The reaction of the electron-rich trisaryloxide complex [(($^{t\text{-Bu}}$ArO)$_3$tacn)U^{III}] (**1**) (($^{t\text{-Bu}}$ArO)$_3$tacn^{3-} = trianion of 1,4,7-tris(3,5-di-*tert*-butyl-2-hydroxybenzyl)-1,4,7-triazacyclononane) with benzophenone yielded intractable products that were not isolable. However, on the basis of literature precedence, we surmised that the reaction may have formed diphenyl methoxide and reductive coupling products. Accordingly, the disubstituted 4,4′-di-*tert*-butylbenzophenone was chosen as an alternative that would provide electronic stabilization of the radical and deter dimerization due to *tert*-butyl groups blocking access to the para and pinacol coupling pathways.

Synthesis and Molecular Structure of 2 and 3. Treating a red-brown hexane solution of [(($^{t\text{-Bu}}$ArO)$_3$tacn)U^{III}] (**1**) with 1 equiv of disubstituted 4,4′-di-*tert*-butylbenzophenone affords a purple precipitate (Scheme 1). The deep purple solids are isolated in good yield (73%) by vacuum filtration and characterized as a U(IV) ketyl radical complex [(($^{t\text{-Bu}}$ArO)$_3$tacn)U^{IV}(OC•$^{t\text{-Bu}}$Ph$_2$)] (**2**). Purple XRD-quality crystals can be obtained from diffusion of acetonitrile into a tetrahydrofuran solution of **2**.

In the presence of neat 1,4-cyclohexadiene, complex **2** undergoes a color change from purple to green within 12 h, indicative of H atom abstraction to form the corresponding U(IV) diphenyl methoxide complex [(($^{t\text{-Bu}}$ArO)$_3$tacn)U^{IV}(OCH$^{t\text{-Bu}}$Ph$_2$)] (**3**). Recrystallization of **3** from pentane results in XRD-quality green single crystals.

The molecular structure of **2** reveals the 4,4′-di-*tert*-butylbenzophenone ketyl fragment nestled inside the reactive pocket at the seventh axial position of the trisaryloxide uranium compound (Figure 1, left). The average U−O(ArO) and U−N(tacn) ligand distances of 2.207 and 2.683 Å, respectively, are comparable to those of precursor complex **1** (Table 1). Note that four resonance structures constitute the overall solid-state molecular structure of complex **2**, with three structures possessing U(IV) oxidation states and one with U(III) oxidation state (Figure 2, **2a**−**2d**). Interestingly, this one U(III) resonance structure determines, to a significant extent, how complex **2** structurally and spectroscopically deviates from that of typical U(IV) 5f^2 complexes. For instance, the U1−O4 bond length of 2.178(4) Å is appreciably longer than that of previously reported U(IV) 5f^2 complexes of the (^{R}ArO)$_3$tacn^{3-} ligand system[37] and of the reported U(IV) aryloxide complex [U^{IV}(OAr)$_4$] (d(U−O)$_{av}$ = 2.136 Å).[38] The bond distance of 1.334(6) Å for the C70−O4 bond is shorter than that of a C−O single bond, indicating that complex **2** may possess an oxidation that is intermediate between U(III) and U(IV). The U1−O4 bond length of 2.178(4) Å and the C70−O4 bond length of 1.334(6) Å is comparable to the bond distances reported for the Sm(III) benzophenone ketyl complex by Domingos et al. where the Sm−O bond is 2.199 Å and the C−O bond is 1.322 Å.[35] In addition, no significant disruptions in aromaticity of the phenyl groups are observed in the molecular structure, most likely due to complex **2** having two resonance structures where the aromaticity remains intact (**2a** and **2d**). A notable feature of the structure of **2** is the sum of the angles around the ketyl carbon, which total up to 359.96°, confirming that ketyl carbon C70 is indeed sp^2-hybridized and that H abstraction has not occurred.

The molecular structure of complex **3** reveals coordination of the diphenyl methoxide ligand at the axial position perpendicular to the trisaryloxide plane (Figure 1, right). The average

(30) Cui, C.; Köpke, S.; Herbst-Irmer, R.; Roesky, H. W.; Noltemeyer, M.; Schmidt, H.-G.; Wrackmeyer, B. *J. Am. Chem. Soc.* **2001**, *123*, 9091–9098.
(31) Deacon, G. B.; Forsyth, C. M.; Wilkinson, D. L. *Chem.—Eur. J.* **2001**, *7*, 1784–1795.
(32) Hou, Z.; Koizumi, T.; Nishiura, M.; Wakatsuki, Y. *Organometallics* **2001**, *20*, 3323–3328.
(33) Villiers, C.; Adam, R.; Lance, M.; Nierlich, M.; Vigner, J.; Ephritikhine, M. *J. Chem. Soc., Chem. Commun.* **1991**, 1144–1145.
(34) Hou, Z.; Jia, X.; Hoshino, M.; Wakatsuki, Y. *Angew. Chem., Int. Ed. Engl.* **1997**, *36*, 1292–1294.
(35) Domingos, Â.; Lopes, I.; Waerenborgh, J. C.; Marques, N.; Lin, G. Y.; Zhang, X. W.; Takats, J.; McDonald, R.; Hillier, A. C.; Sella, A.; Elsegood, M. R. J.; Day, V. W. *Inorg. Chem.* **2007**, *46*, 9415–9424.
(36) Clegg, W.; Eaborn, C.; Izod, K.; O'Shaughnessy, P.; Smith, J. D. *Angew. Chem., Int. Ed. Engl.* **1997**, *36*, 2815–2817.
(37) Castro-Rodriguez, I.; Meyer, K. *Chem. Commun.* **2006**, 1353–1368.
(38) Berg, J. M.; Clark, D. L.; Huffman, J. C.; Morris, D. E.; Sattelberger, A. P.; Streib, W. E.; Sluys, W. G. V. D.; Watkin, J. G. *J. Am. Chem. Soc.* **1992**, *114*, 10811–10821.

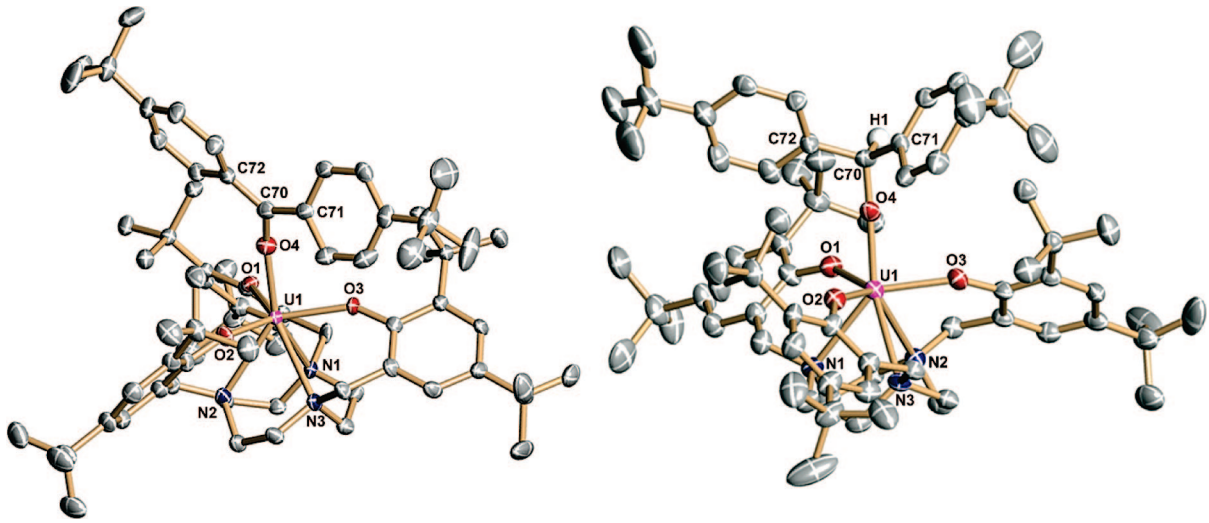

Figure 1. Molecular structures of [(($^{t\text{-Bu}}$ArO)$_3$tacn)U^{IV}(OC•$^{t\text{-Bu}}$Ph$_2$)] (**2**) (left) in crystals of **2**·3C$_4$H$_8$O and of [(($^{t\text{-Bu}}$ArO)$_3$tacn)U^{IV}(OCH$^{t\text{-Bu}}$Ph$_2$)] (**3**) (right) in crystals of **3**·C$_6$H$_6$/CH$_3$CN. Thermal ellipsoids are at the 50% probability level. Hydrogens (except H1) and co-crystallized solvent molecules are omitted for clarity.

Table 1. Selected Structural Parameters for Complexes **2**, **3**, **6**, and **7** (Bond Distances in Angstroms, Angles in Degrees)

structural parameters	2	3	6	7
U1−N1$_{tacn}$	2.698(4)	2.673(4)	2.646(3)	2.717(6)
U1−N2$_{tacn}$	2.700(4)	2.706(4)	2.704(3)	2.643(6)
U1−N3$_{tacn}$	2.652(4)	2.678(4)	2.688(3)	2.706(5)
U1−N$_{av}$	2.683	2.686	2.678	2.689
U1−O1$_{ArO}$	2.208(3)	2.218(3)	2.216(3)	2.196(5)
U1−O2$_{ArO}$	2.217(3)	2.228(3)	2.233(2)	2.221(4)
U1−O3$_{ArO}$	2.197(3)	2.192(3)	2.200(3)	2.213(4)
U1−O$_{av}$	2.207	2.213	2.215	2.210
U1−O4	2.178(4)	2.077(3)	2.092(3)	2.168(4)
U2−O8				2.109(4)
C70−O4	1.334(6)	1.406(5)	1.386(5)	1.366(7)
C71−O8				1.423(7)
U1−O4−C70	159.6(3)	178.4(3)	171.9(3)	160.2(4)
U2−O8−C71				167.6(4)
Σ∠ C$_{ketyl}$	359.96			
U$_{out\text{-}of\text{-}plane\ shift}$	−0.232	−0.216	−0.163	−0.163/4

ligand U−O(ArO) and U−N(tacn) distances in the molecular structure of **3** remain unperturbed at 2.213 and 2.686 Å, respectively. The U1−O4 bond distance of 2.077(3) Å and the C70−O4 distance of 1.406(5) Å in complex **3** are appreciably different than those of **2**. The shorter U1−O4 bond of 2.077(3) Å is indicative of stronger U−L electrostatic interaction in complex **3** than in **2** and is in agreement with the U−O distance reported for the only other known U(IV) diphenylmethoxide complex (2.071 Å).[19] In addition, the U1−O4−C70 angle of 178.4(3)° in **3** is close to linear, whereas the U1−O4−C70 angle of **2** is bent at an angle of 159.6(3)°.

Defined as the displacement of the uranium atom below the triangular plane of the three phenolic oxygens, the uranium out-of-plane shift (U_{oop}) is an important structural parameter in complexes of the [((^{R}ArO)$_3$tacn)U] system because it provides an indication of metal−ligand interaction strength.[37] This parameter, which is a function of U−L orbital involvement and electrostatic interaction, decreases as the formal oxidation state of the uranium ion increases. For instance, the uranium out-of-plane shift (U_{oop}) for the six-coordinate precursor complex **1** is −0.75 Å. With strongly bound axial ligands, such as in complexes **2** and **3**, U_{oop} values shift to −0.232 and −0.216 Å, respectively. In comparison, the uranium ion in **3** is pulled more toward the plane than in **2**, indicating that **3** has better U−L orbital involvement and is consistent with **2** having the U(III) resonance structure (**2d**). Also, compound **2** has a much longer U1−O4 bond and shorter C70−O4 bond (Figure 3) than **3**, again in compliance with **2** having the U(III) resonance structure (**2d**). It should be noted that such a feature can also be attributed to the delocalization of the negative charge of the ketyl radical species. In view of the two resonance structures, where the single electron resides on the *ortho*- and *para*-carbons (**2b** and **2c**), the C70−C$_{Ar}$ bonds are expected to be shorter in **2** than in **3**, and indeed that is observed in the structural parameters of **2**. The structural differences between **2** and **3** clearly indicate that **2** deviates from typical U(IV) 5f^2 complexes.

Electronic Structure of 2 and 3. In order to elucidate the electronic structure of complexes **2** and **3**, Kohn−Sham DFT calculations were performed on complexes using the ADF package (2007.01).[39,40] Key geometry parameters are summarized in Table 2, and DFT isosurface plots are shown (Figures 4 and 6).[41,42] The experimental and computed distances agree remarkably well and show only very small deviations of about 0.02 Å.

The core of complex **3** has an idealized C_3 symmetry with a strong methoxy oxygen ligator coordinating along the *z*-axis. From a ligand field point of view, it is expected that methoxide complex **3** behaves like an f^2 system, in which the set of seven f orbitals are antibonding with respect to the filled orbitals of the ligands. A scaled ZORA computation on **3** revealed that SOMO and SOMO′ are mainly of f character and can be assigned to orbitals f$_{xyz}$ and f$_{z(x^2-y^2)}$ (Figure 4). In accordance with ligand field theory, the f$_{xyz}$ and f$_{z(x^2-y^2)}$ orbitals have δ symmetry with respect to the U−O axis and contain the two f electrons since they have only weak π interactions with the aryloxide oxygens and no interaction with the methoxide group

(39) te Velde, G.; Bickelhaupt, F. M.; Gisbergen, S. J. A. v.; Guerra, C. F.; Baerends, E. J.; Snijders, J. G.; Ziegler, T. *J. Comput. Chem.* **2001**, *22*, 931–967.
(40) Guerra, C. F.; Snijders, J. G.; te Velde, G.; Baerends, E. J. *Theor. Chem. Acc.* **1998**, *99*, 391.
(41) Laaksonen, L. *J. Mol. Graphics* **1992**, *10*, 33.
(42) Bergman, D. L.; Laaksonen, L.; Laaksonen, A. *J. Mol. Graphics Modelling* **1997**, *15*, 301.

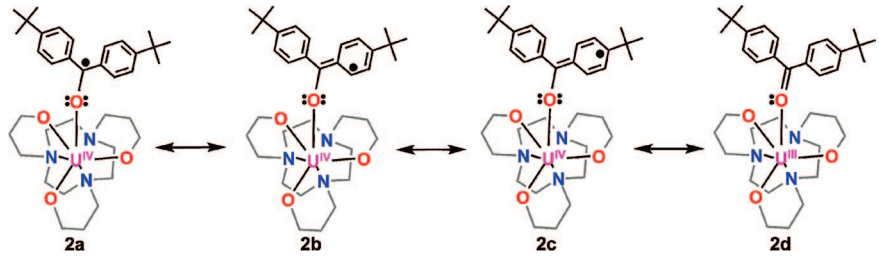

Figure 2. Resonance structures of complex **2**, **2a**−**2d**.

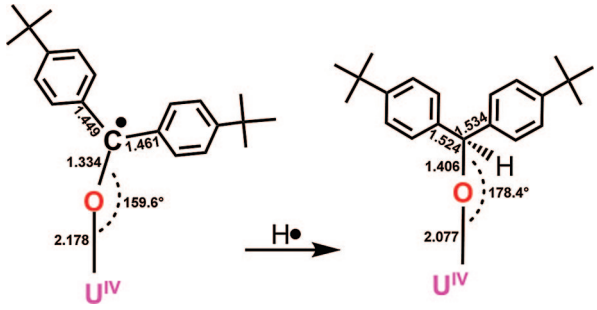

Figure 3. Comparison of selected bond distances of complexes **2** and **3**.

Table 2. Comparison of Computed (DFT) and Actual Bond Lengths (XRD) for Complexes **2** and **3** (Bond Distances in Angstroms, Angles in Degrees)

structural parameters	2	computed 2	3	computed 3
U1−N_{av}	2.683	2.733	2.700	2.763
U1−O_{av}	2.207	2.217	2.215	2.228
U1−O4	2.178	2.190	2.080	2.105
C70−O4	1.334	1.328	1.385	1.414
U1−O4−C70	159.6	159.9	175.5	175.7

(Figure 5). The $f_{y(y^2-3x^2)}$ and $f_{x(x^2-3y^2)}$ orbitals are 3-fold φ symmetry with respect to the U−O axis and are well matched for σ and π antibonding overlaps with ligands in the aryloxide plane. Hence, these orbitals lie higher in energy and are empty. The next two higher energy orbitals, f_{xz^2} and f_{yz^2} (π antibonding), and the highest orbital, f_{z^3} (σ antibonding), are also empty.

The total spin density plot of U(IV) f^2 complex **3** confirms that the f_{xyz} and $f_{z(x^2-y^2)}$ orbitals indeed carry the main part of the spin; however, a small spin polarization on the coordinated

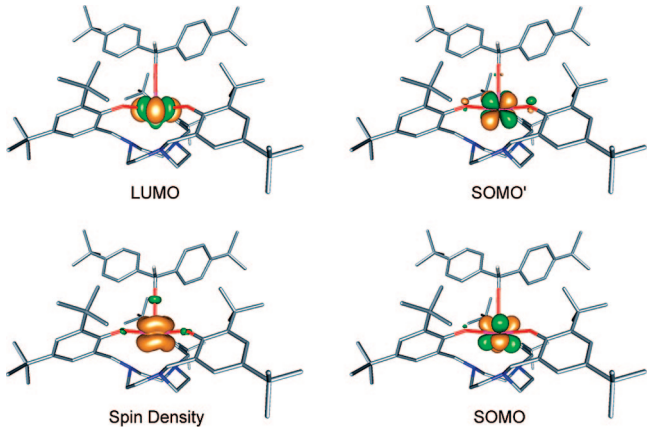

Figure 4. DFT isosurface contour plots featuring the two degenerate SOMOs (right), the LUMO (top left), and the resulting spin density (bottom left) of [((*t*-BuArO)$_3$tacn)U^{IV}(OCH*t*-BuPh$_2$)] (**3**).

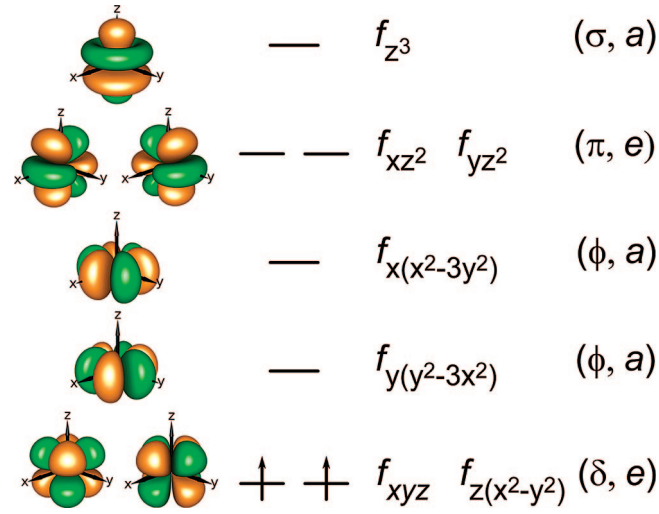

Figure 5. Ligand-field f orbital splitting diagram of **3**, an f^2 system with an idealized C_3 symmetry and a strong axial ligand.

ligand is observed. Such a spin polarization on the ligand is often observed for high valent transition metal complexes.[43]

In C_3 symmetry, each of the seven f orbitals are either totally symmetric (a) or part of a degenerate pair (e). The two π orbitals transform together and form one e set. The two δ orbitals also transform together and form another e set. The z^3 is unchanged under a 120° turn and thus is totally symmetric in C_3. The φ orbitals [$y(y^2-3x^2)$ and $x(x^2-3y^2)$] are also unchanged under a 120° turn (refer to figure) and, thus, also totally symmetric in C_3. Since the φ orbitals do not transform together, they may have individual energies. Their chemical difference is also apparent since one φ orbital has perfect σ overlap with the ligands in the plane, while the other has perfect π overlap with them.

The ketyl radical complex **2** was modeled to have three unpaired electrons by computing it as a U(III) complex. However, the resulting orbitals and spin density plot suggest a more complex representation (Figure 6). SOMO-2 and SOMO-1, of δ-type f_{xyz} and $f_{z(x^2-y^2)}$, are similar to the SOMOs of the U(IV) complex **3** and are purely uranium f orbital in character. Conversely, SOMO is not simply a pure uranium f orbital but rather only 25.8% uranium based (24.0% f and 1.8% d); the remaining Mulliken AO occupation of the orbital is ligand based. The uranium contribution of the orbital is an f_{z^3} directionally optimized for π overlap with the ligand carbonyl oxygen π orbitals. The ligand contribution shows density exactly where

(43) Astashkin, A. V.; Neese, F.; Raitsimring, A. M.; Cooney, J. J. A.; Bultman, E.; Enemark, J. H. *J. Am. Chem. Soc.* **2005**, *127*, 16713–16722.

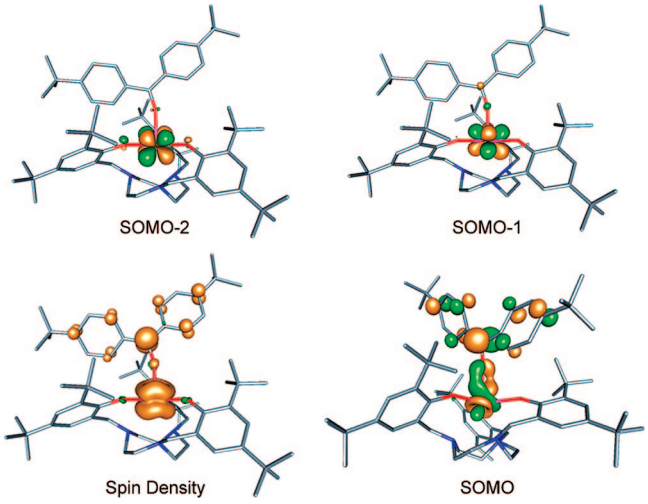

Figure 6. DFT isosurface contour plots featuring SOMO-1 and SOMO-2 of metal character (top), the lowest energy SOMO of mainly ligand character (bottom right), and the resulting spin density (bottom left) of [(($^{t\text{-Bu}}$ArO)$_3$tacn)U^{IV}(OC•$^{t\text{-Bu}}$Ph$_2$)] (**2**).

one would expect for a reduced diphenyl ketone, that is, mainly on the ketyl carbon and on the *ortho*- and *para*-carbon atoms in the phenyl rings. Spin and charge densities confirm the intermediate oxidation state of the uranium center. The Mulliken charge on the uranium of 1.46 is between those found for the precursor complex [(($^{t\text{-Bu}}$ArO)$_3$tacn)U^{III}] (**1**) (1.04) and the U(IV) methoxide complex **3** (1.61). Likewise, the spin densities of complex **2** (2.37) is between that of complex **1** (3.11) and **3** (2.17). The intermediate oxidation state of the uranium ion may explain the shift to the UV region of uranium based $5f^3$ to $5f^26d^1$ transitions commonly observed in the visible region of the electronic absorption spectra of the [((^{R}ArO)$_3$tacn)U^{III}] system, which give rise to their red-brown color.[44,45] This agreement between structural, spectroscopic, and the computational data of these complexes verifies that the scaled ZORA computation correctly reflects the electronic structure of complex **2**.

The DFT calculations have further affirmed that the charge-separated species is stabilized by a high degree of resonance and agrees well with structural parameters found in the molecular structure of complex **2**. The spin density map of complex **2** displays the delocalization of the single unpaired electron throughout the ligand, including ortho and para positions of the axial ligand's phenyl rings. In addition, one-third of the electron has been found to reside on the uranium metal center, confirming the resonance structures proposed for **2** in Figure 2. The U1−O4−C70 angle of ketyl complex **2** is significantly more bent (159.6°) than that of the methoxide complex **3** (178.4°) and can be attributed to a significant contribution of the U(III) resonance structure (**2d**) to the overall molecular structure of **2** (Figure 2).

Magnetism of 2 and 3. Variable temperature magnetization data were measured on two independently synthesized samples. The data of complex **2** show a steady drop in μ_{eff} as the temperature is lowered, decreasing from 3.48 μ_B at 300 K to 1.61 μ_B at 5 K. Complexes of U(IV) ($5f^2$) commonly show a variable temperature magnetization trace that exhibits a μ_{eff} range from ~0.5 μ_B at 4 K to ~3.0 μ_B at 300 K.[37] The reduction

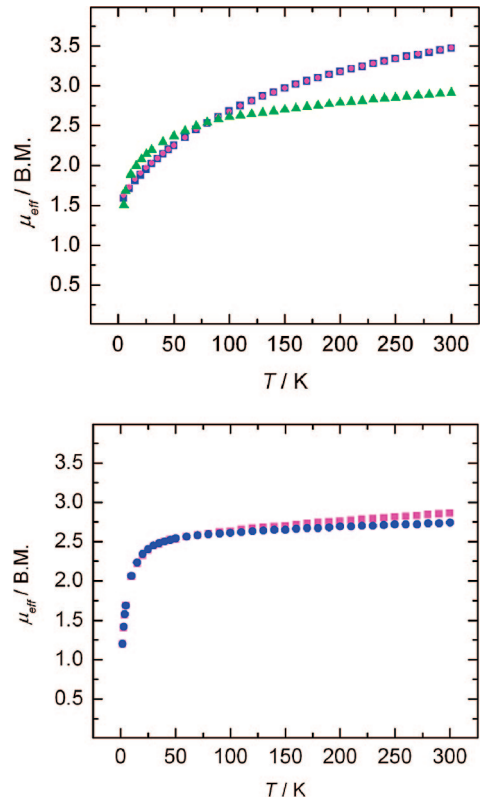

Figure 7. Temperature-dependent SQUID magnetization data (1 T) for complex **2** (top) plotted as magnetic moment (μ_{eff}) versus temperature (T) (blue and magenta) along with uranium CO_2 radical anion complex [((^{Ad}ArO)$_3$tacn)U^{IV}($CO_2^{\bullet-}$)] for comparison (green). The data for complex **3** is also shown (bottom). Data were corrected for diamagnetism, and reproducibility was checked on multiple independently synthesized samples.

in magnetic moment at low temperatures is consistent with a poorly isolated singlet ground state arising from ligand field effects.[46] The higher magnetic moment at low temperatures of **2** (5 K, μ_{eff} = 1.61 μ_B) is unusual and is likely due to magnetic contributions from the single unpaired electron residing on the disubstituted benzophenone ligand fragment as well as from the U(III) resonance structure (**2d**) as previously discussed (Figure 7, top). The room temperature magnetic moment is higher (300 K, μ_{eff} = 3.48 μ_B) than that found in most U(IV) $5f^2$ complexes. This is consistent with the DFT calculations, in which one-third of the single radical electron is located on the uranium, hence, raising the magnetic moment. The low temperature magnetic behavior of **2** is similar to that of the η^1-bound uranium CO_2 complex [((^{Ad}ArO)$_3$tacn)U^{IV}($CO_2^{\bullet-}$)] previously reported,[47] which has also been characterized as a charge-separated U(IV) complex containing a radical anionic ligand. In conclusion, magnetization studies reveal that complex **2** is no ordinary U(IV) $5f^2$ complex and should be viewed in its own class spectroscopically as a charge-separated U(III)−L ↔ U(IV)−L$^{\bullet-}$ $5f^3$ ↔ $5f^2$ complex.

In contrast, the magnetization data of complex **3** reveal a temperature dependency that is much different than that of **2**, keeping in accordance with other U(IV) $5f^2$ of the (^{R}ArO)$_3$tacn ligand system bearing closed-shell axial ligands.[37] The low temperature magnetic moment for complex **3** (μ_{eff} = 1.14−2.81

(44) Karbowiak, M. *J. Phys. Chem. A* **2005**, *109*, 3569–3577.
(45) Karbowiak, M.; Drozdzyński, J. *J. Phys. Chem. A* **2004**, *108*, 6397–6406.
(46) Stewart, J. L.; Andersen, R. A. *New J. Chem.* **1995**, *19*, 587–595.
(47) Castro-Rodriguez, I.; Nakai, H.; Zakharov, L. N.; Rheingold, A. L.; Meyer, K. *Science* **2004**, *305*, 1757–1759.

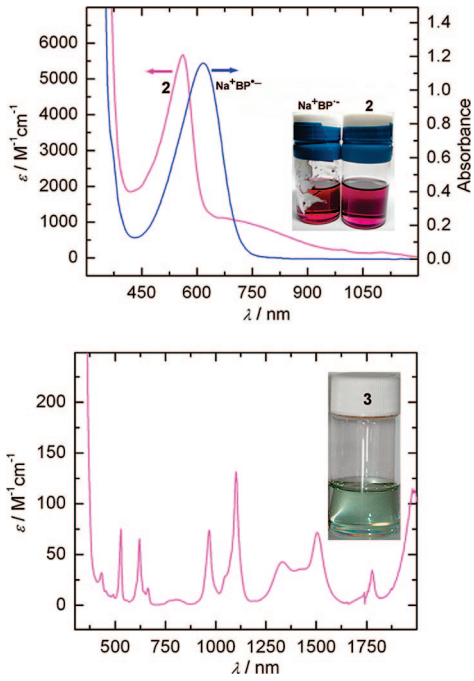

Figure 8. Electronic absorption spectrum of **2** in toluene (top, magenta) plotted as extinction coefficient (ϵ) versus wavelength (λ) along with the spectrum of the sodium benzophenone ketyl radical (blue). The spectrum of **3** in toluene is also shown (bottom).

μ_B, 2−300 K) is lower than that of complex **2** (Figure 7, bottom) but still higher than most [((^{R}ArO)$_3$tacn)U^{IV}(L)] complexes, which usually exhibit a magnetic moment of 0.5 μ_B at 5 K.[37] This could be due to compound **3** possessing magnetic states lying closer together in energy than others and, thus, get populated faster at lower temperatures. The general temperature dependence and room temperature moment of 2.81 μ_B is typical for most U(IV) 5f^2 complexes but strays from theoretical values calculated for a ^{3}H$_4$ ground state $\mu_{eff} = g_j(J(J+1))^{1/2} = 3.58$ μ_B. This can be attributed to the quenching of spin−orbit coupling of uranium complexes leading to a reduced magnetic moment. Accordingly, U(IV) complexes typically have low observed magnetic moment compared to theoretical values.

Electronic Absorption of 2 and 3. The majority of the U(IV) complexes of the trisaryloxide ligand system, reported in the past, have appeared as pale green solids, almost colorless in appearance. Hence, the isolation of a deep purple powder immediately indicates the formation of the uranium ketyl radical complex similar to the Na-ketyl radical produced for the solvent drying and deoxygenation process. The electronic absorption spectrum of **2** in toluene features an intense absorption band (λ_{max} = 562 nm, ϵ = 5680 M^{-1} cm^{-1}) in the visible region (Figure 8, top). This absorption gives rise to the ketyl complex's distinctive and intense purple color and is assigned to the $\pi-\pi^*$ transition of a highly conjugated ketyl system. The transition energy of 562 nm is blue-shifted from that of the sodium benzophenone ketyl radical, which exhibits the $\pi-\pi^*$ transition at 618 nm. The shift of λ_{max} to a higher energy wavelength upon coordination to the uranium metal has also been observed with previously reported metal ketyl radical complexes.[16,17] The electronic absorption spectrum of the sodium benzophenone ketyl radical is similar to those reported in the literature.[13,48]

The pale green color of complex **3** signifies the loss of extended conjugation of the π system present in ketyl complex **2** due to H abstraction. Consequently, the electronic absorption spectrum of **3**, recorded in toluene, shows the disappearance of the $\pi-\pi^*$ transition from the visible region of the electromagnetic spectrum. Instead, only weak f−f transitions commonly observed for lanthanide and actinide complexes remain, scattered throughout the NIR region (Figure 8, bottom).[49] The UV/vis/NIR spectrum of **3** compares well with reported U(IV) complexes[38,50] and demonstrates that electronic absorption spectroscopy is diagnostic of oxidation state and 5f^n electron configuration.

Synthesis and Molecular Structure of 6 and 7. In light of the difficulties of isolating the benzophenone ketyl radical complex with the ($^{t\text{-Bu}}$ArOH)$_3$tacn ligand system, we attempted to stabilize the unsubstituted benzophenone ketyl radical by using amoresterically encumbering adamantyl derivatized ligand (^{Ad}ArO)$_3$-tacn^{3-} (trianion of 1,4,7-tris(3-adamantyl-5-*tert*-butyl-2-hydroxybenzyl)-1,4,7-triazacyclononane). Treating a red-brown frozen benzene solution of trivalent [((^{Ad}ArO)$_3$tacn)U^{III}] (**4**) with 1 equiv of benzophenone results in an intense purple color that persists for ~15 s after the solution is thawed before turning greenish-brown. As judged from its intense colorization, this transient species is presumably a uranium benzophenone ketyl radical complex [((^{Ad}ArO)$_3$tacn)U^{IV}(OC•Ph$_2$)] (**5**) formed from an intramolecular single-electron reduction of benzophenone by U(III) (Scheme 2) analogous to that seen in the formation of complex **2**. Similarly, the intense purple color is attributed to the $\pi-\pi^*$ transition of the highly conjugated benzophenone ketyl radical ligand fragment (λ_{max} = 550 nm) and is comparable to that of the purple sodium benzophenone ketyl radical in toluene (λ_{max} = 624 nm) (Figure 9). Allowing the reaction to proceed for 12 h yields a green solution. From this solution, green solids are isolated by solvent evaporation, and single crystals suitable for X-ray diffraction were obtained from diffusion of acetonitrile into a benzene solution. The molecular structure analysis reveals a U(IV) diphenylmethoxide complex [((^{Ad}ArO)$_3$tacn)U^{IV}(OCHPh$_2$)] (**6**) (Figure 1) similar to **3**. One possible source of hydrogen atom stems from complex decomposition, which also might explain the low isolated yield of 57%. Complex **6** can be reproduced in significantly higher yield when the reaction is done in the presence of hydrogen sources, such as THF, 1,4-cyclohexadiene, or R$_3$Sn−H (isolated 75% yield).

X-ray diffraction study of **6** reveals a seven-coordinate uranium complex. The coordination sphere displays the uranium center encased almost entirely by the macrocyclic hexadentate ligand, leaving only the seventh axial coordination site available, where the ligand binds roughly perpendicular to the trisaryloxide plane. The average U−O(ArO) and U−N(tacn) distances of 2.216 and 2.679 Å (Table 1) are consistent with other U(IV) complexes of the [((^{R}ArO)$_3$tacn)U^{IV}(L)]-type.[37] The U1−O4 and C70−O4 bond lengths of 2.092(3) and 1.386(5) Å in **6**, respectively, are in good agreement with compound **3**. For reference, the uranium out-of-plane shift for the six-coordinate starting complex **4** is U_{oop} = −0.88 Å. The uranium out-of-plane shift for **6** of −0.163 Å is a significant shift from the six-coordinate U(III) complex, which is consistent with the strong binding of the methoxide ligand to a highly oxophilic uranium center. The U1−O4−C70 angle in **6** of 171.9(3)° is

(48) Kawai, A.; Hirakawa, M.; Abe, T.; Obi, K.; Shibuya, K. *J. Phys. Chem. A* **2001**, *105*, 9628–9636.
(49) Marks, T. J. *Progress in Inorganic Chemistry*; John Wiley & Sons: New York, 1979; Vol. 25.
(50) Berg, J. M.; Sattelberger, A. P.; Morris, D. E. *Inorg. Chem.* **1993**, *32*, 647–653.

Scheme 2. Formation of Diphenyl Methoxide Complex **6** and Para-Coupling Dimeric Complex **7** through Intermediate Ketyl Complex **5** from a One-Electron Reduction of Benzophenone by a U(III) Precursor Complex [((^{Ad}ArO)$_3$tacn)U^{III}] (**4**)

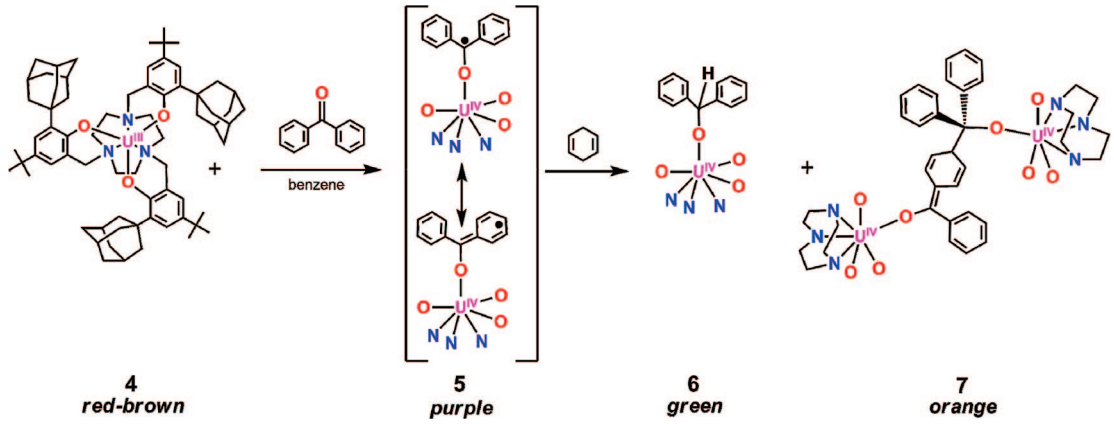

similar to that seen in **3** of 178.4(3)°. Overall, the metrics of **6** are reminiscent of those of **3**; this is expected since both complexes have similar electronic structures.

In addition to the formation of complex **6** from the reaction of **4** with benzophenone, dinuclear complex [((^{Ad}ArO)$_3$tacn)U^{IV}-(OCPhPh−CPh$_2$O)U^{IV}((^{Ad}ArO)$_3$tacn)] (**7**) also forms as a crystalline byproduct in low yield (5%) (Figure 10). Single crystals suitable for XRD studies of **7** were obtained from slow diffusion of acetonitrile into a toluene solution of crude **6**. Evidently, the formation of **7** results from head-to-tail para coupling of ketyl radical complex **5**. In **7**, where U1 bears the sp^2-hybridized C70, the U1−O4 bond of 2.168(4) Å and the O4−C70 bond length of 1.366(7) Å are reminiscent of complex **2**. The U2 in **7** bears the sp^3-hybridized C71 and correspondingly the U2−O8 bond of 2.109(4) Å and O8−C71 bond length of 1.423(7) Å are reminiscent of complex **3**. Breaking of aromaticity can be observed in the nonplanar bridged ring, where there are four long single bonds and two short double bonds. Complex **7** represents the first structurally characterized product resulting from para coupling of two benzophenone ketyl radical species. Pinacol coupling is typically preferred for ketyls; however, there are a few cases where para coupling takes preference due to steric demands,[9,51] such is the case here with the bulky adamantyl groups in the [((^{Ad}ArO)$_3$tacn)U^{III}] system.

Conclusion

Stabilization and structural characterization of a uranium benzophenone ketyl radical complex were accomplished by employing the sterically demanding (^{R}ArO)$_3$tacn ligand system. It has been demonstrated in previous works that the [((^{R}ArO)$_3$tacn)U^{III}) system can stabilize highly reactive charge-separated uranium complexes.[47,52] These charge-separated complexes containing radical anionic ligands are appreciated because they are rare and spectroscopically interesting and, due to their highly reactive nature, have the potential to undergo further chemistry.[52] Isolating and probing the electronic structures of these charge-separated complexes are therefore important endeavors if one wants to understand and control reactivity. Structural characterization of the ketyl radical complex [(($^{t\text{-}Bu}$ArO)$_3$tacn)U^{IV}(OC•$^{t\text{-}Bu}$Ph$_2$)] (**2**) along with DFT calculations have provided us more insight into the reactivity

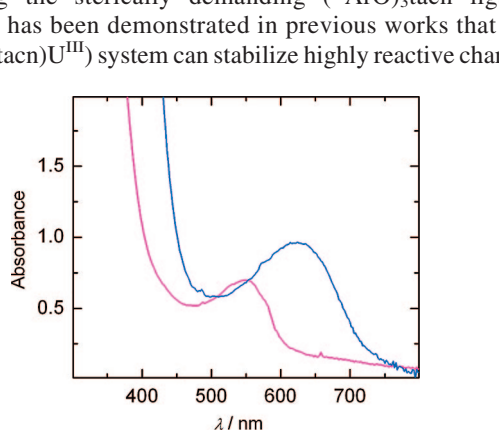

Figure 9. Electronic absorption spectrum of ketyl intermediate complex **5** (magenta) and sodium benzophenone ketyl (blue).

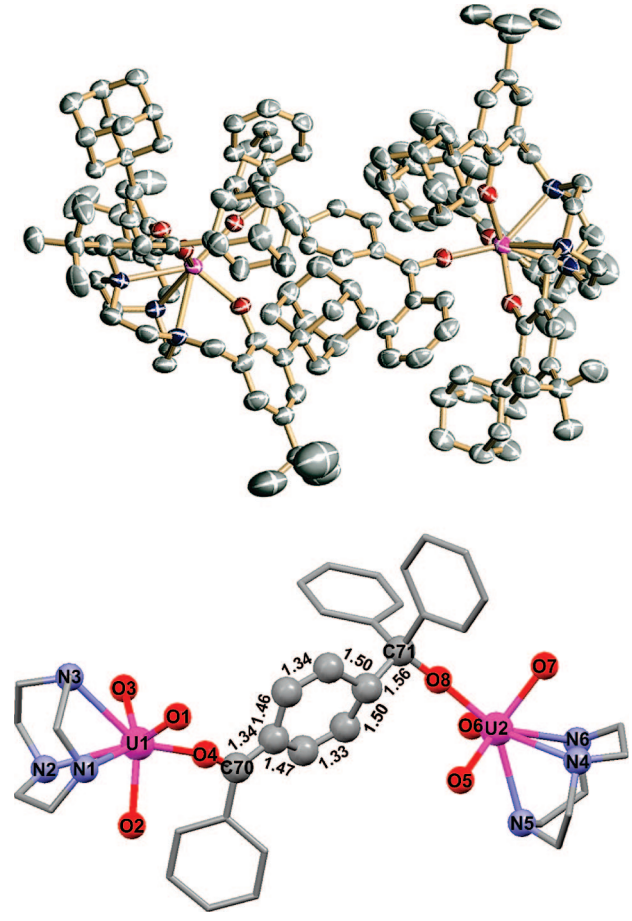

Figure 10. Molecular structure of complex **7** in crystals of **7**·6 CH$_3$CN/5 C$_7$H$_8$ (top) and the core with selected bond lengths (bottom). Thermal ellipsoids are at the 35% probability level. Hydrogens and co-crystallized solvent molecules are omitted for clarity.

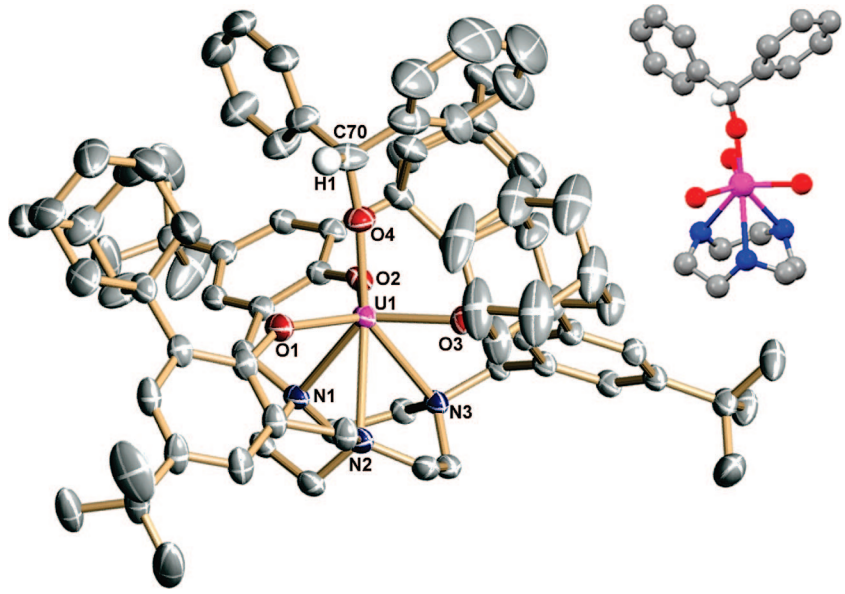

Figure 11. Molecular structure of [((^{Ad}ArO)$_3$tacn)U^{IV}(OCHPh$_2$)] (**6**) in crystals of **6**·CH$_3$CN/0.5 C$_6$H$_6$. Thermal ellipsoids are at the 35% probability level. Hydrogens (except H1) and co-crystallized solvent molecules are omitted for clarity.

of the [((^{R}ArO)$_3$tacn)U^{III}] system. In addition to examining the reactivity of complex **2**, we also plan to isolate and study other charge-separated complexes containing radical anions. We are currently investigating a wide variety of ligands with different sterics in hopes of achieving the delicate balance between stabilizing these highly reactive complexes and promoting controlled reactivity.

Experimental Section

General Methods. All experiments were performed under dry nitrogen atmosphere using standard Schlenk techniques or an MBraun inert gas glovebox. Solvents were purified using a two-column solid-state purification system (Glasscontour System, Irvine, CA) and transferred to the glovebox without exposure to air. NMR solvents were obtained from Cambridge Isotope Laboratories, degassed, and stored over activated molecular sieves prior to use.

Methods. Magnetism data of crystalline powdered samples (20−30 mg) were recorded with a SQUID magnetometer (Quantum Design) at 10 kOe (5−300 K for **2** and **6** and 2−300 K for **3**). Values of the magnetic susceptibility were corrected for the underlying diamagnetic increment ($\chi_{dia} = -986.01 \times 10^{-6}$ cm^3 mol^{-1} (**2**), -988.94×10^{-6} cm^3 mol^{-1} (**3**), -885.84×10^{-6} cm^3 mol^{-1} (**6**)) by using tabulated Pascal constants and the effect of the blank sample holders (gelatin capsule/straw). Samples used for magnetization measurement were recrystallized multiple times and checked for chemical composition and purity by elemental analysis (C, H, and N) and ^{1}H NMR spectroscopy. Data reproducibility was also carefully checked on independently synthesized samples.

^{1}H NMR spectra were recorded on JEOL 270 and 400 MHz instruments operating at respective frequencies of 269.714 and 400.178 MHz with a probe temperature of 23 °C in C$_6$D$_6$. Chemical shifts were referenced to protio solvent impurities (δ 7.15 (C$_6$D$_6$)) and are reported in parts per million.

Electronic absorption spectra were recorded from 200 to 2000 nm (Shimadzu (UV-3101PC)) in the indicated solvent.

Results from elemental analysis were obtained from the Analytical Laboratories at the Friedrich-Alexander-University Erlangen-Nürnberg (Erlangen, Germany) on Euro EA 3000.

Kohn−Sham DFT calculations were performed on complexes **2** and **3** using the ADF package (2007.01). Analyses and geometry optimizations of the complexes were performed employing the BP86 gradient corrected functional[53–55] in the scalar zeroth-order regular approximation (ZORA[56–58]). The basis set applied is of TZP quality with frozen cores for the second row elements (1s) and for uranium (including 5d). In the ZORA computation, the α and β spin densities are the sum of all densities of the α and β spin−orbitals, respectively. The spin density plots are obtained by taking the difference between the α and the β spin densities. ADF input files are provided in the electronic Supporting Information.

Starting Materials. [(THF)$_4$UI$_3$] and [U(N(SiMe$_3$)$_2$)$_3$] were prepared as described by Clark et al.[59–61] Uranium turnings were purchased from Oak Ridge National Laboratory (ORNL) and activated according to literature procedures. Benzophenone (98%) was purchased from Aldrich and used as received after appropriate degassing procedures. 4,4′-Di-*tert*-butylbenzophenone was synthesized according to literature procedures.[62]

Complex Synthesis. [(($^{t\text{-Bu}}$ArO)$_3$tacn)U^{IV}(OC•$^{t\text{-Bu}}$Ph$_2$)] (2). To a red-brown hexane solution (6 mL) of [(($^{t\text{-Bu}}$ArO)$_3$tacn)U^{III}] (**1**) (200 mg, 0.196 mmol) was added 4,4′-di-*tert*-butylbenzophenone (57.7 mg, 0.196 mmol) with stirring. Immediately, purple precipitate formed in a purple solution. The reaction was stirred at room temperature for 1 h. The purple solids were isolated by vacuum filtration and washed with small amounts of hexane and dried under vacuum. Recrystallization by diffusion of acetonitrile into a tetrahydrofuran solution afforded purple single crystals as **2**·3C$_4$H$_8$O (yield 188 mg, 0.143 mmol, 73%): ^{1}H NMR (290 MHz, benzene-

(51) Maury, O.; Villiers, C.; Ephritikhine, M. *Tetrahedron Lett.* **1997**, *38*, 6591–6594.
(52) Lam, O. P.; Feng, P. L.; Heinemann, F. W.; O'Connor, J. M.; Meyer, K. *J. Am. Chem. Soc.* **2008**, *130*, 2806–2816.
(53) Becke, A. D. *Phys. Rev. A* **1988**, *38*, 3098.
(54) Perdew, J. P. *Phys. Rev. B* **1986**, *33*, 8822.
(55) Perdew, J. P. *Phys. Rev. B* **1986**, *34*, 7406.
(56) Lenthe, E. V.; Baerends, E. J.; Snijders, J. G. *J. Chem. Phys.* **1993**, *99*, 4597.
(57) Lenthe, E. V.; Baerends, E. J.; Snijders, J. G. *J. Chem. Phys.* **1994**, *101*, 9783.
(58) Lenthe, E. V.; Ehlers, A. E.; Baerends, E. J. *J. Chem. Phys.* **1999**, *110*, 8943.
(59) Avens, L. R.; Bott, S. G.; Clark, D. L.; Sattelberger, A. P.; Watkin, J. G.; Zwick, B. D. *Inorg. Chem.* **1994**, *33*, 2248–2256.
(60) Clark, D. L.; Sattelberger, A. P.; Andersen, R. A. *Inorg. Synth.* **1997**, *31*, 307–315.
(61) Clark, D. L.; Sattelberger, A. P.; Bott, S. G.; Vrtis, R. N. *Inorg. Chem.* **1989**, *28*, 1771–1773.
(62) Gibson, H. W.; Lee, S.-H.; Engen, P. T.; Lecavalier, P.; Sze, J.; Shen, Y. X.; Bheda, M. *J. Org. Chem.* **1993**, *58*, 3748–3756.

d_6, 20 °C) δ = 69.06 (d, 2H, $\Delta\nu_{1/2}$ = 50.4 Hz), 32.17 (s, 6H, $\Delta\nu_{1/2}$ = 65.7 Hz), 8.45 (s, 18H (*t*-Bu H's on BP), $\Delta\nu_{1/2}$ = 33.1 Hz), 0.96 (d, 9H, $\Delta\nu_{1/2}$ = 30.5 Hz), −1.29 (s, 3H, $\Delta\nu_{1/2}$ = 27.1 Hz), −2.38 (s, 3H, $\Delta\nu_{1/2}$ = 30.4 Hz), −2.57 (s, 27H (2-*t*-Bu H's), $\Delta\nu_{1/2}$ = 29.7 Hz), −3.13 (s, 3H, $\Delta\nu_{1/2}$ = 28.6 Hz), −4.61 (s, 2H, $\Delta\nu_{1/2}$ = 25.9 Hz), −6.43 (s, 27H (4-*t*-Bu H's), $\Delta\nu_{1/2}$ = 44.3 Hz), −7.21 (s, 1H, $\Delta\nu_{1/2}$ = 33.2 Hz), −10.11 (s, 2H, $\Delta\nu_{1/2}$ = 40.5 Hz), −19.42 (s, 1H, $\Delta\nu_{1/2}$ = 33.8 Hz). Anal. Calcd for **2**: C, 65.83; H, 7.98; N, 3.20. Found: C, 65.81; H, 7.99; N, 3.37.

[(($^{t\text{-Bu}}$ArO)$_3$tacn)U^{IV}(OCH$^{t\text{-Bu}}$Ph$_2$)] (3). Stirring a purple solution of [(($^{t\text{-Bu}}$ArO)$_3$tacn)U^{IV}(OC•$^{t\text{-Bu}}$Ph$_2$)] (**2**) (200 mg, 0.152 mmol) in neat 1,4-cyclohexadiene (1.5 mL) for 12 h resulted in a cloudy green solution with a small amount of fine light-gray precipitate. The light-gray precipitate was filtered off leaving a light-green solution. The filtrate was evaporated to dryness under reduced pressure and dried in vacuo. Recrystallization from a concentrated pentane solution produced green block crystals suitable for X-ray diffraction as **3**•C_5H_{12} (yield 140 mg, 0.106 mmol, 70%): ^{1}H NMR (290 MHz, benzene-d_6, 20 °C) δ = 51.88 (s, 3H, $\Delta\nu_{1/2}$ = 38.1 Hz), 50.47 (s, 3H, $\Delta\nu_{1/2}$ = 6.6 Hz), 15.94 (d, 3H, $\Delta\nu_{1/2}$ = 7.2 Hz), 5.57 (s, 6H, $\Delta\nu_{1/2}$ = 4.5 Hz), 3.97 (s, 9H (*t*-Bu H's on BP), $\Delta\nu_{1/2}$ = 3.8 Hz), 3.69 (s, 9H (*t*-Bu H's on BP), $\Delta\nu_{1/2}$ = 4.0 Hz), 2.53 (s, 1H, $\Delta\nu_{1/2}$ = 3.3 Hz), 2.47 (s, 6H, $\Delta\nu_{1/2}$ = 5.1 Hz), 1.13 (s, 3H, $\Delta\nu_{1/2}$ = 2.5 Hz), −4.64 (s, 27H (2-*t*-Bu H's), $\Delta\nu_{1/2}$ = 3.3 Hz), −6.95 (s, 3H, $\Delta\nu_{1/2}$ = 5.5 Hz), −7.41 (s, 3H, $\Delta\nu_{1/2}$ = 4.5 Hz), −8.11 (s, 2H, $\Delta\nu_{1/2}$ = 26.9 Hz), −16.09 (s, 27H (4-*t*-Bu H's), $\Delta\nu_{1/2}$ = 13.4 Hz). Anal. Calcd for **3**: C, 65.78; H, 8.05; N, 3.20. Found: C, 65.67; H, 8.08; N, 3.34.

[((^{Ad}ArO)$_3$tacn)U^{IV}(OCHPh$_2$)] (6). A benzene solution (0.5 mL) of benzophenone (29 mg, 0.16 mmol) was added to a thawing benzene solution (10 mL) of [((^{Ad}ArO)$_3$tacn)U^{III}] (**4**) (200 mg, 0.16 mmol) while stirring. The reaction was allowed to stir at room temperature for 4 h. Green solids were isolated by solvent evaporation. Recrystallization of the green powder by slow diffusion of acetonitrile into a benzene solution produces single rectangular shaped crystals of **6**•CH_3CN/0.5 C_6H_6. The crystals can be isolated by filtration and dried in vacuo to obtain the bulk solid (yield 120 mg, 0.084 mmol, 52%). Alternatively, **6** can also be synthesized in higher yields by doing the reaction of [((^{Ad}ArO)$_3$tacn)U^{III}] (**4**) (100 mg, 0.08 mmol) with benzophenone (15 mg, 0.08 mmol) in neat 1,4-cyclohexadiene (6 mL). After 12 h, the green reaction solution is filtered and evaporated to dryness. The crude solids are washed with hexane and dried (yield 85 mg, 0.06 mmol, 75%): ^{1}H NMR (400 MHz, benzene-d_6, 20 °C) δ = 45.95 (d, 4H, $\Delta\nu_{1/2}$ = 24.7 Hz), 5.83 (d, 6H, $\Delta\nu_{1/2}$ = 25.1 Hz), 3.23 (d, 6H, $\Delta\nu_{1/2}$ = 21.4 Hz), 2.26 (s, 9H, $\Delta\nu_{1/2}$ = 8.5 Hz), 1.21 (d, 4H, $\Delta\nu_{1/2}$ = 8.55 Hz), 1.18 (m, 12H, $\Delta\nu_{1/2}$ = 6.05 Hz), 0.91 (d, 3H, $\Delta\nu_{1/2}$ = 1.11 Hz), 0.84 (t, 12H, $\Delta\nu_{1/2}$ = 1.42 Hz), 0.05 (s, 3H, $\Delta\nu_{1/2}$ = 1.05 Hz), −3.49 (s, 3H, $\Delta\nu_{1/2}$ = 2.55 Hz), −4.17 (s, 27H (*t*-Bu H's), $\Delta\nu_{1/2}$ = 2.51 Hz), −4.48 (s, 3H, $\Delta\nu_{1/2}$ = 2.52 Hz), −5.16 (s, 6H, $\Delta\nu_{1/2}$ = 26.8 Hz), −5.29 (s, 3H, $\Delta\nu_{1/2}$ = 10.2 Hz), −26.78 (s, 6H, $\Delta\nu_{1/2}$ = 25.4 Hz).

Crystallographic Details. Crystallographic details for **2**: Purple prismatic crystals grown from slow diffusion of acetonitrile into a tetrahydrofuran solution at room temperature were coated with Paratone N oil on a microscope slide. A crystal of approximate dimensions 0.36 × 0.25 × 0.20 mm^3 was selected and mounted on a nylon loop. A total of 67 965 reflections ($-18 \le h \le 18$, $-22 \le k \le 22$, $-36 \le l \le 36$) were collected at T = 100(2) K in the θ range from 3.42 to 26.37°, of which 15 959 were unique (R_{int} = 0.0844) and 11 992 were observed [$I > 2\sigma(I)$] on a Bruker-Nonius KappaCCD diffractometer using Mo Kα radiation (λ = 0.71073 Å). The structure was solved by direct methods (SHELXTL NT 6.12, Bruker AXS, Inc., 2002). All non-hydrogen atoms were refined anisotropically. Hydrogen atoms were placed in calculated idealized positions. One of the *t*-butyl groups (C59−C62) of the ligand is subjected to rotational disorder around C59. Two preferred orientations have been refined resulting in occupancies of 74(2)% for C60−C62 and 26(2)% for C60A−C62A. One of the THF molecules is also disordered. Two preferred orientations have been refined, resulting in occupancies of 82.5(8)% for O7−C84 and 17.5(8)% for O7A−C84A. SAME restraints were applied in the refinement of the THF molecules. Additional SIMU restraints were applied in the refinement of the disordered THF. The residual peak and hole electron densities were 1.966 and −2.954 e•Å^{-3}. The absorption coefficient was 2.123 mm^{-1}. The least-squares refinement converged normally with residuals of R_1 = 0.0726, wR_2 = 0.1273, and GOF = 1.098 (all data). $C_{84}H_{128}N_3O_7U$, monoclinic, space group $P2_1/c$, a = 14.794(2), b = 18.245(2), c = 29.226(4) Å, β = 96.198(7)°, V = 7842(2) Å^3, Z = 4, ρ_{calcd} = 1.296 mg/m^3, $F(000)$ = 3204, $R_1(F)$ = 0.0480, $wR_2(F^2)$ = 0.1138 [$I > 2\sigma(I)$]. CCDC reference number: 676962.

Crystallographic details for **3**: Green rectangular shaped crystals grown from slow diffusion of acetonitrile into benzene at room temperature were coated with Paratone N oil on a microscope slide. A crystal of approximate dimensions 0.29 × 0.28 × 0.27 mm^3 was selected and mounted on a nylon loop. A total of 101 493 reflections ($-13 \le h \le 12$, $-33 \le k \le 33$, $-62 \le l \le 62$) were collected at T = 150(2) K in the θ range from 3.24 to 26.37°, of which 14 880 were unique (R_{int} = 0.0465) and 10 662 were observed [$I > 2\sigma(I)$] on a Bruker-Nonius KappaCCD diffractometer using Mo Kα radiation (λ = 0.71073 Å). The structure was solved by direct methods (SHELXTL NT 6.12, Bruker AXS, Inc., 2002). All non-hydrogen atoms were refined anisotropically. Hydrogen atoms were placed in calculated idealized positions. Two of the *t*-butyl groups are disordered. Two alternative positions have been refined in each case, resulting in site occupancies of 56(2) and 44(2)% for C19−C21 and C19A−C21A and of 82(2) and 18(2)% for C60−C62 and C60A−C62A, respectively. SIMU, ISOR, and SADI restraints were applied in the refinement of one of these *t*-butyl groups (C59, C60−C62, C60A−C62A). The residual peak and hole electron densities were 1.256 and −1.669 e•Å^{-3}. The absorption coefficient was 2.266 mm^{-1}. The least-squares refinement converged normally with residuals of R_1 = 0.0748, wR_2 = 0.0809, and GOF = 1.173 (all data). $C_{80}H_{114}N_4O_4U$, orthorhombic, space group $Pbca$, a = 10.772(2), b = 27.180(3), c = 50.052(4) Å, V = 14654(3) Å^3, Z = 8, ρ_{calcd} = 1.300 mg/m^3, $F(000)$ = 5968, $R_1(F)$ = 0.0484, $wR_2(F^2)$ = 0.0750 [$I > 2\sigma(I)$]. CCDC reference number: 676963.

Crystallographic details for **6**: Green rectangular shaped crystals grown from slow diffusion of acetonitrile into benzene at room temperature were coated with Paratone N oil on a microscope slide. A crystal of approximate dimensions 0.30 × 0.27 × 0.25 mm^3 was selected and mounted on a nylon loop. A total of 61 689 reflections ($-18 \le h \le 18$, $-29 \le k \le 28$, $-29 \le l \le 29$) were collected at T = 150(2) K in the θ range from 2.92 to 27.10°, of which 16 197 were unique (R_{int} = 0.0325) and 12 987 were observed [$I > 2\sigma(I)$] on a Bruker SMART diffractometer using Mo Kα radiation (λ = 0.71073 Å). The structure was solved by direct methods (SHELXTL NT 6.12, Bruker AXS, Inc., 2002). All non-hydrogen atoms were refined anisotropically. Hydrogen atoms were placed in calculated idealized positions. One of the *t*-butyl groups is disordered. Two alternative positions have been refined resulting in site occupancies of 73.8(8) and 26.2(8)% for C31−C33 and C31A−C33A, respectively. SIMU restraints were applied in the refinement of two further *t*-butyl groups where no disorder could be resolved. The residual peak and hole electron densities were 2.762 and −1.497 e•Å^{-3}. The absorption coefficient was 2.252 mm^{-1}. The least-squares refinement converged normally with residuals of R_1 = 0.0493, wR_2 = 0.1078, and GOF = 1.063 (all data). $C_{87}H_{113}N_4O_4U$, monoclinic, space group $P2_1/n$, a = 14.5176(8), b = 22.682(2), c = 23.334(2) Å, β = 106.046(1)°, V = 7384.3(7) Å^3, Z = 4, ρ_{calcd} = 1.364 mg/m^3, $F(000)$ = 3148, $R_1(F)$ = 0.0384, $wR_2(F^2)$ = 0.1046 [$I > 2\sigma(I)$]. CCDC reference number: 676964.

Crystallographic details for **7**: Orange rectangular shaped crystals grown from slow diffusion of acetonitrile into toluene at room temperature were coated with Paratone N oil on a microscope slide. A crystal of approximate dimensions 0.30 × 0.25 × 0.10 mm^3

was selected and mounted on a nylon loop. A total of 69 300 reflections ($-22 \le h \le 22$, $-23 \le k \le 23$, $-35 \le l \le 35$) were collected at $T = 100(2)$ K in the θ range from 2.94 to 27.10°, of which 35 321 were unique ($R_{int} = 0.0521$) and 24 345 were observed [$I > 2\sigma(I)$] on a Bruker SMART diffractometer using Mo Kα radiation ($\lambda = 0.71073$ Å). The structure was solved by direct methods (SHELXTL NT 6.12, Bruker AXS, Inc., 2002). All non-hydrogen atoms were refined anisotropically. Hydrogen atoms were placed in calculated idealized positions. Two of the *t*-butyl groups of the ligand are disordered. Two alternative positions each have been refined to give occupancies of 53(1)% for C25−C27 and 47(1)% for C25′−C27′ and of 82(1)% for C107−C109 and 18(1)% for C167−C169. The crystal structure contains a total of 4 molecules of NCMe and 2.625 molecules of toluene, a number of which is disordered. The disordered parts include sharing of alternative positions for toluene or NCMe molecules only but also sharing of a site between a toluene and an NCMe. SIMU and ISOR restraints have been applied in modeling the disordered parts of the structure. Detailed occupancies and further information can be taken from the deposited data. The residual peak and hole electron densities were 1.898 and −1.430 e·Å^{-3}. The absorption coefficient was 2.017 mm^{-1}. The least-squares refinement converged normally with residuals of $R_1 = 0.0973$, $wR_2 = 0.1504$, and GOF = 1.065 (all data). $C_{190.38}H_{245}N_{10}O_8U_2$, triclinic, space group $P\bar{1}$, $a = 17.321(4)$, $b = 18.075(4)$, $c = 28.033(7)$ Å, $\alpha = 102.643(3)$, $\beta = 90.799(3)$, $\gamma = 104.456(3)$°, $V = 8271(3)$ Å^3, $Z = 2$, $\rho_{calcd} = 1.316$ mg/m^3, $F(000) = 3411$, $R_1(F) = 0.0606$, $wR_2(F^2) = 0.1360$ [$I > 2\sigma(I)$]. CCDC reference number: 676965.

Acknowledgment. Special thanks to Arnie Rheingold, Peter Gantzel, and Antonio DiPasquale for help with the crystal structures. This work was funded by DOE Grant DE-FG02-O4ER 15537, SFB583, and DFG. We thank the GAAN Fellowship Program for support of O.P.L. This research was also supported in part by NSF Grant CHE05-18707 (J.M.O.). K.M. congratulates Professor Bernt Krebs (Uni Münster) and dedicates this paper on the occasion of his 70th birthday.

Supporting Information Available: ADF input files. This material is available free of charge via the Internet at http://pubs.acs.org.

JA801007Q